



HAL
open science

On the groove pressing of Ni-W alloy: microstructure, texture and mechanical properties evolution

S. Koriche, S. Boudekhani-Abbas, H. Azzeddine, K. Abib, A-L Helbert, F. Brisset, T. Baudin, D. Bradai

► To cite this version:

S. Koriche, S. Boudekhani-Abbas, H. Azzeddine, K. Abib, A-L Helbert, et al.. On the groove pressing of Ni-W alloy: microstructure, texture and mechanical properties evolution. *Kovove materialy [Metallic materials]*, 2018, 56 (05), pp.313-323. 10.4149/km_2018_5_313 . hal-02359938

HAL Id: hal-02359938

<https://hal.science/hal-02359938>

Submitted on 11 Dec 2019

HAL is a multi-disciplinary open access archive for the deposit and dissemination of scientific research documents, whether they are published or not. The documents may come from teaching and research institutions in France or abroad, or from public or private research centers.

L'archive ouverte pluridisciplinaire **HAL**, est destinée au dépôt et à la diffusion de documents scientifiques de niveau recherche, publiés ou non, émanant des établissements d'enseignement et de recherche français ou étrangers, des laboratoires publics ou privés.

On the Groove pressing of Ni-W alloy: Microstructure, texture and mechanical properties evolution

Siham Koriche¹, Saadia Boudekhani-Abbas¹, Hiba Azzeddine^{1,2,*}, Khadidja Abib¹,
Anne-Laure Helbert³, Francois Brisset³, Thierry Baudin³, Djamel Bradai¹

¹ Faculty of Physics, University of Sciences and Technology HouariBoumediene, BP 32 El-Alia, 16111, Algiers, Algeria.

² Departments of Physics, University Mohamed Boudiaf, BP 166, 28000, M'Sila Algeria

³ ICMMO, SP2M, Univ. Paris-Sud, Université Paris-Saclay, UMR CNRS 8182, 91405 Orsay Cedex, France

Abstract

The microstructure, texture and mechanical properties of the Ni-14%W(wt.%) alloy with two different initial grain sizes and textures were investigated after groove pressing (GP) at 450 °C to 4 cycles using Electron Back Scatter Diffraction (EBSD) and microhardness measurements. The initial first series was characterized by small equiaxed grains and Cube dominant texture component. The second series has elongated grains and β -fiber texture. EBSD analysis has shown that GP processing led to a slight refinement (less than 15%) of equiaxed grains in series I while greater refinement (~55%) of the mean spacing along normal direction was observed in series II. The texture did not drastically change from the initial ones and was characterized by the weakening of the Cube component in series I and rapid decrease of Copper component for series II. GP processing reduces very slightly the plastic anisotropy of the alloy with initial elongated granular microstructure.

Keywords: SPD, Groove Pressing, Ni-W alloy, Microstructure, Texture, plastic anisotropy

* Corresponding author: Dr. Hiba AZZEDDINE, E-mail: azehibou@yahoo.fr

Departments of Physics, University Mohamed Boudiaf, BP 166, 28000, M'Sila Algeria

1. Introduction

Recently, Ni based alloys rouse a great interest due to their potential applications as coated conductor substrates for superconducting cables. Especially, Ni-5at.%W (14 wt. %) has been in the focus of many investigations and can be considered as the most applied material for Rolling Assisted Biaxially Textured Substrates (RABITS™) [1]. Among their most desired properties are: special texture, temperature stability, low lattice constant misfit; mechanical strength, price and availability. They exhibit excellent physical properties subsequently to easy forming of Cube {001}<100> texture after heavy straining and subsequent annealing [2, 3]. This Cube texture is prerequisite for obtaining thin layers with high conversion efficiency. The amount of Cube-oriented grains depends strongly on the deformation texture and microstructure that may result from prior thermo-mechanical processing [4]. Therefore, conventional processing techniques such as rolling and severe plastic deformation (SPD) processing like accumulative roll bonding (ARB) were experimented in order to investigate their effect on the microstructure and texture development [5–9]. Recently, Gupta et al. [10] stated that the Groove pressing (GP) technique is one of the most suitable SPD techniques for fabricating sheet materials having very interesting mechanical and physical properties. Basically, in GP process, sheet material is subjected to repetitive shear deformation under the plane strain deformation conditions by alternately pressing between asymmetrically grooved and flat dies [11]. Different existing types of groove pressing methods as constrained groove pressing, unconstrained groove pressing (or simply groove pressing), semi-constrained groove pressing, rubber pad-constrained groove pressing, constrained groove pressing-cross route and covered sheet casing-constrained groove pressing. All these methods have the same principle as the groove pressing that

involves alternatively corrugating and flattening of the sheet specimens [9]. Materials processed by CGP exhibit very high strength, high hardness and many other desirable properties. Profuse data has been published concerning different materials like aluminum, copper, low carbon steel, nickel, etc. [9].

Sunil et al. [12] studied the wettability and corrosion resistance of groove pressed AZ31 magnesium alloy and showed the prospects in its application as implants instead of expensive titanium. Potential industrial applications of the CGPed materials based on the research that has been done till now is widely discussed in [10].

Most studies were devoted to highlight the effect of CGP processing on mechanical properties and microstructural evolution in face centered cubic metals like Copper and Aluminum [11–17] but little on Nickel [18, 19]. However, very few studies were carried out on the evolution of crystallographic texture [20, 21] and any on the variation of grain boundary character distribution (GBCD) after GP processing.

The GP process has several advantages, such as ultrafine grain microstructures in metals and its applicability to thin sheet materials, which cannot be applied to the most widely used SPD processes like ECAP [22].

It is a good challenge to investigate whether GP processing (replacing conventional cold rolling) could enhance the volume fraction of Cube texture as well as ensures good formability of Ni-14W (wt.%) alloy that is potential candidate as conductor substrate. The main point is that GP processing does not require huge processing to achieve equivalent properties obtained through cold rolling or ARB.

Therefore, in the present study, the deformation microstructure, texture as well mechanical properties of a commercial Ni-14W (wt.%) alloy with two different initial

grain morphologies and textures were investigated after GP) at 450 °C to 4 cycles using Electron Back Scatter Diffraction (EBSD) and microhardness measurements.

2. Experimental techniques

The material investigated in the present work is a commercial Ni-14W (wt. %) alloy (kindly provided by APERAM alloys society, France) in the form of strips of 1 mm thickness. The Chemical composition of Ni-14W (wt. %) alloy is presented in Table 1. The material was received in two different initial granular morphologies: equiaxed and elongated for series I and II, respectively.

The strips were cut into 35 mm × 20 mm × 1 mm rectangular pieces and then degreased in acetone. The strips were pressed between asymmetrically grooved dies (with a groove angle of 45° and width of 4 mm, Fig. 1a) and then subsequently between flat die (Fig. 1b). As a result of pressing and straightening, the length of the specimen increased. The strip was then rotated 180° around normal direction, allowing the un-deformed regions to be deformed by further pressings (Figs. 1c-1d). The pressing was performed on a commercial BeraTest™ hydraulic press with a maximum load of 2000 KN at a constant speed. The successive pressings by grooved dies and flat dies result in an even distribution of plastic strain throughout the work-piece. Before each press stage, the strips were preheated at 450°C for 5 minutes. The entire process corresponds to one GP cycle. We have used a slightly modified groove pressing in the sense where a CCW 45° rotation around the normal direction (ND) direction was applied to the sample between successive cycles. A total of 4 GP cycles was successfully obtained.

The microstructure and texture were investigated using Electron Back Scatter Diffraction (EBSD) in the (Rolling Direction (RD)-Normal Direction (ND)) cross-

section of sample after a mechanically and electro polishing using the A2 Struers electrolyte at 25 V. The observation was carried out using a scanning electron microscope FEG-SEM SUPRA 55 VP operating at 20 kV. The EBSD step size was 50 nm. EBSD data acquisition and analysis were conducted using the TSL Orientation Imaging Microscopy, OIMTM software. The quantitative texture analysis was carried out by calculating the Orientation Distribution Function (ODF) using MTEX software [23]. The microhardness of the material was measured after each GP cycle using a Shimadzu G21 series with a diamond pyramid indenter under loading charge of 2.94 N and indentation time of 10 seconds. An average of 20 readings was taken near the middle of the sample to obtain the average micro-hardness value.

3. Results and discussion

3.1. Microstructure and texture of Ni-W alloy before GP processing

The orientation imaging micrographs (OIM) in inverse pole figure (IPF map) obtained from the two initial states of Ni-14W alloy are illustrated in Fig.2. The initial microstructure of the series I is characterized by equiaxed grains with small average size ($d \sim 6.5\mu\text{m}$). Twins (as shown by arrows) are profuse and are extended through several grains. Meanwhile, the series II exhibited an elongated morphology resulting from the rolling process, with mean spacing along normal direction (ND) about $1.8\mu\text{m}$.

Fig. 3 shows the misorientation distributions of the series I and II of as received Ni-14W alloy. It is clear that both samples do not exhibit a random distribution. The grain boundaries are classified into two categories based on the misorientation between the neighboring grains. They are low-angle boundaries (LAGBs) when misorientation is $5^\circ \leq \theta \leq 15^\circ$, and high-angle boundaries (HAGBs) when the misorientation angle is $\theta > 15^\circ$.

Special grain boundaries are selected often in the range $\Sigma 3$ - $\Sigma 27$ [7]. The misorientation histogram of series I (Fig. 3a) confirms the presence of great fraction of twins near 60° angle ($\Sigma 3$ $60^\circ/\langle 111 \rangle$) while series II exhibit a high fraction (near 50 %) of low angle grain boundaries resulted from the generation of dislocations during rolling deformation.

The initial texture of both as received of Ni-14W alloys are shown in Fig. 4. The main ideal texture component positions of FCC alloys are also presented and their descriptions are given in Table 2. The initial texture of series I was characterized as relatively weak recrystallization type texture with the presence of dominant Cube $\{001\}\langle 100 \rangle$ component. A very weak intensity of the S $\{231\}\langle 346 \rangle$ and the Copper $\{112\}\langle 111 \rangle$ components can be noticed. Contrarily, the initial texture of series II was characterized by the presence of Brass $\{011\}\langle 211 \rangle$, Copper $\{112\}\langle 111 \rangle$ and S $\{123\}\langle 634 \rangle$ component as a pure metal or Copper-type deformation texture (characteristic of pure FCC metals with high stacking fault energy) in which orientations are assembled along the β -fibre (that spreads from Brass $\{011\}\langle 112 \rangle$ to Copper $\{112\}\langle 111 \rangle$ through S $\{231\}\langle 634 \rangle$ components).

3.2. Microstructure and texture evolution of Ni-W alloy after GP processing

3.2.1. Microstructure evolution of Ni-W alloy after GP processing

The IPF maps of series I and II of Ni-14W alloy after GP processing up 4 cycles are shown in Fig.5. The evolution of misorientation angles for both initial states as function of GP processing are illustrated in Fig.6.

A lack of substantial refinement can be noticed in the microstructure of series I upon GP processing (Fig. 5) while the refinement seems effective for the second series. A close

analysis of Fig. 6a evidences a decrease of $\Sigma 3$ (twin) fraction and increase of low disorientation angles due to the increase of deformation level (dislocations) for series I. A strict reverse trend is noticed for series II. The low angle grain boundary (LAGB) fraction decreases as the high angle grain boundary (HAGB) one increases.

The grain size and fraction of HAGB are shown in Fig.7 for both initial states of Ni-14W alloy after GP processing. As it can be seen, the grain size of series I decreases slightly from 6.5 to 4.5 μm after four GP cycles. While, series II exhibits a greater refinement ($\sim 55\%$) where the mean spacing along ND decreases from 1.8 μm to 0.6 μm after 4 GP cycles with no saturation. It is to be noted that the length of the elongated grains, i.e mean spacing along RD was not considered since it overflows the analyzed zone along RD. It has been already reported that the initial equiaxed grain size was reduced from 78 μm to a cell block structure approximately 0.5 μm for Copper and from 38 μm to 1 μm for aluminium after three and four cycles of CGP processing, respectively [15, 17]. Moreover, Wang et al. [20] evidenced a strong refinement of initial equiaxed grains ($\sim 28 \mu\text{m}$) that became elongated subgrains with mean width (mean spacing along normal direction) of about 0.5 μm through CGP processing pure Ni at room temperature up to four cycles. This considerable grain refinement was ascribed to the intermediate value of stacking fault energy (SFE) [20]. The SFE of pure Ni at room temperature was estimated to be about 128 mJ/m^2 [24, 25]. The temperature dependence of the SFE $d\gamma_{SFE}/dT$ was estimated to be $-0.04 \text{ mJ}/\text{m}^2 \text{ K}$ for pure Ni [25]. It is worth noting that no similar data does exist for Ni-14W alloy, but one can speculate that the temperature dependence of SFE should be close. Nevertheless, the SFE of Ni-5W alloy must be significantly lower than that of pure Ni due to alloying of Ni with 5 at.% W, since SFE tends to decrease with segregation [26].

Kumar et al. [18] have assumed that CGP processing resulted in lower grain refinement compared to other SPD techniques. In fact, alternate groove pressing and flattening operations is accompanied by a reversal of loading direction which results in the non-existence of multiple shear stress planes during deformation and partial annihilation of dislocations. Moreover, in the present study, the groove angle of 45° may introduce small strain in the material.

From Fig. 7, the volume fraction of HAGB for series I decreases substantially from 80% after 1GP cycle to 53 % after 4 GP cycles. In fact, the decrease of HAGB fraction is associated to the increase of LAGB caused by the imposed deformation and generation of new dislocations while for series II, it increases faintly from 22 % after 1 GP to saturate around 35% after 3 GP cycles. Apparently, in series II, the LAGBs progressively rotate to HAGBs with strain, which is a characteristic of grain refinement mechanism in FCC metals [5, 27, 28].

3.2.1 Texture evolution of Ni-W alloy after GP processing

The ODF sections ($\varphi_2 = 0, 45$ and 65°) of series I and II of Ni-14W alloy after GP processing are presented in Fig.8. For more details, the evolution of β and θ -fibre are plotted for both series in Fig.9.

It can be seen that the texture after GP processing is similar to that of as received alloys. No new components have been developed for both Ni-14W alloys. As can be shown in Figs. 8 and 9a, the intensity of Cube component of series I shows a continuous decrease with increasing number of GP cycles and seem to re-increase after four GP cycles (4.4 mrd).

As shown in Fig. 9b, the intensity Copper component decreases rapidly after 1 GP cycle and levels off with increasing GP cycles. It can be observed that the intensity of Brass component does not seem to be systematically higher than that of Copper component and/or increases after GP processing which should be an indication of the formation of a Brass-type texture. The texture transition from Copper-type to Brass-type texture has been widely reported in FCC alloys of low stacking fault energy after conventional plastic deformation [29]. A similar transition occurs in copper–manganese alloys [30] and in age-hardened aluminium alloys [31]. It has been suggested that the texture transition in FCC alloys is a result of the onset of planar slip and shear banding [29]. Sarma et al. [32] have demonstrated that a two-step recrystallization annealing was beneficial in achieving a strong cube texture in Ni–W alloys up to 14wt.%. However the Cube fraction was found to decrease with W content above 5 at.%. This was attributed to the transition in the rolling texture from Copper-type to Brass-type with increasing W content. In agreement with Sarma et al. [32], the absence of texture transition in the Ni-5W alloy (with relatively low W content) after GP processing could be associated with its probable high stacking fault energy that ensures typical copper or metal type rolling texture.

It was reported that the resulted texture during CGP processing of pure Ni sheets at room temperature depend strongly on the design of groove dies, specially the groove width and angle [20]. A rotated cube component $\{1\ 0\ 0\}\langle 0\ 1\ 1\rangle$ is developed from the initial Cube texture $\{1\ 0\ 0\}\langle 0\ 0\ 1\rangle$ of the annealed Ni sheets when using groove dies with a width of 3 mm and an angle of 45°. While, no texture change (stable Cube texture) was observed when using groove dies with a width of 2 mm and an angle of 37 or 45° [18]. The present results are close to this last case, with no rotation of the Cube

component towards Rotated-Cube one due to the use of groove dies with a width of 4 mm and an angle of 45°. This different behavior may be explained by the effect of solute elements (W) and processing temperature (here 450 °C) on the texture components formation and/or re-orientation. Indeed, it is well known that increasing solute element content decreases the stacking fault energy that in turn, determines the texture of FCC metals [23].

3.3. Evolution of the microhardness

The evolution of Vickers microhardness of Ni-14W alloy after GP processing of the two series is presented in Fig. 10. The microhardness behaves quite differently depending on the initial state. The improvement of the microhardness of the series I was as high as 30% (Hv~ 220 of as received alloy and Hv ~318 after 4GP cycles). That of series II was more modest and reached no more than 10% (Hv~ 331 of as received alloy and Hv ~ 347 after 4 GP cycles).

In the literature, many authors reported substantial hardening of the studied materials after CGP processing. Pure Ni [20] and Al [33], experienced high hardening level up to 140 and 80 %, respectively after four cycles at room temperature [20]. Constrained groove pressing of low carbon steel at room temperature revealed also 100% increasing of the microhardness relatively to initial un-deformed state [34]. Mg alloys (AZ31) were characterized by relatively lower hardening level about 30 % after processing at 450°C [35, 36].

Often, the high hardening level is ascribed to the concomitant effect of grain refinement and dislocations density increase. In the present study, in both samples with different initial microstructure, the increase of the microhardness could be attributed solely to the

net increase of dislocation density in absence of any considerable grain refinement [6, 37] for series I. In Fig.10, series I, it is observed that Hv values increases but with a rate that decreases upon enhancing the accumulated strain. Such evolution has been already evidenced in the literature and quite similar trends were registered for many alloy systems and severe plastic deformation methods [6, 27, 28, 38–42]. Between one and 3 GP cycles, strain hardening mechanisms operate leading to the increase of dislocation density. After reaching a certain level, a second antagonist mechanism of recovery may occur and counterbalance the dislocation generation by their annihilation.

3.4. Evolution of the deep drawability

Since there is strong lack of published data on the influence of SPD on some properties such as fracture behavior, deep drawability and electrical resistivity [9], the deep drawability of the presently studied alloy after GP processing was measured through the variation of plastic anisotropy in GP samples. In this purpose, the Lankford coefficient, R-value, was calculated from the experimental texture (ODFs) of GP processed samples (Fig.9) on the basis of Hosford-Backhofen model implemented in popLA package (<http://www.lanl.gov>). The textured materials are in general anisotropic, so the average Lankford factor \bar{R} and its variation ΔR given by Kocks et al. [43] were used:

$$\bar{R} = \frac{(R(0) + 2R(45) + R(90))}{4} \quad (1)$$

$$\Delta R = \frac{(R(0) - 2R(45) + R(90))}{2} \quad (2)$$

It should be mentioned that for a plastically isotropic material (random texture) R and ΔR should be near unity and zero respectively.

Fig.11 presents the evolution of R value versus the angle to rolling direction corresponding to experimental textures of GP processed samples for both initial states. It is visible that with the increase of the number of GP cycles, the normal anisotropy does not change considerably for series I while it somewhat increases for series II. Between the 1 to 3 GP cycles, the R varied with direction in the strip and is lowest along the RD and TD directions. It increased towards 45° indicating the presence of planar anisotropy.

The evolution of \bar{R} and ΔR versus number of GP cycles is presented in Fig. 12. The \bar{R} and absolute ΔR of the series I were quasi constant, those of series II decreased with increase of number of GP, showing that the sheets became more isotropic. This result showed that GP processing reduces very slightly the plastic anisotropy of the Ni-14W alloy processed by groove pressing with initial elongated granular microstructure.

A number of techniques have been attempted to improve the R value of an FCC metal like aluminum by altering the texture. Improvements of R , \bar{R} and ΔR values of the groove pressed Pure Al sheet were obtained due to the development of (11 1)//ND shear texture [43]. In the present study, the absence of a net texture sharpening around a component or fibre like in Al sheet should explain the weak deep drawability answer of Ni-14W alloy after GP processing at 450 °C.

Continuing research activity is undertaken in order to improve the grain refinement and mechanical properties through processing with dies having lower width and angle and groove pressing at lower temperature than 450 °C.

4. Conclusion

The effect of GP processing at 450 °C for 4 cycles on the microstructure , texture and mechanical properties evolution of Ni-14%W alloy with two different initial grain sizes and textures have been investigated. Based on the present results, following conclusions have been drawn:

- GP at 450°C up to 4 cycles led to a slight refinement of the microstructure.
- The evolution of fraction of HAGB after GP processing strongly depends on the initial microstructure.
- The texture after GP processing did not drastically changed from the initial texture and was characterized by the weakening of the Cube component in series I while Copper component decreases rapidly after 1 GP for series II without texture transition to Brass type.
- An improvement of the microhardness of series I as high as 30% was achieved while that of series II was more modest and reached no more than 10%.
- GP processing reduces slightly the plastic anisotropy of the Ni-14W alloy processed by groove pressing with initial elongated granular microstructure but has no effect on series I.
- Better grain refinement, strengthening of the material and enhancing deep drawability should be better achieved through GP processing at temperature lower than 450 °C and with die width less than 4 mm.

Acknowledgements

The authors are deeply grateful to Yanick ATEBA-BETANDA and Thierry WAECKERLE from APERAM-alloys Imphy Society, France, for kindly providing the

Ni-W alloy. This work was supported by the international PHC-MAGHEB program No. 16MAG03.

References

- [1] Witte, M.: Texture Optimization of Ni-5at.%W for Coated Conductor Application. Diss. RWTH Aachen University, 2013.
- [2] Zhao, Y., Suo, H. L., Liu, M., Liu, D., Zhang, Y., Zhou, M.: *Physica C*, 440, 2006, p. 10.
- [3] Bhattacharjee, P.P., Ray, R.K.: *Mater. Sci. Eng. A*, 459, 2007, p. 309.
- [4] Zaefferer, S., Baudin, T., Penelle, R.: *Acta Mater.*, 49, 2001, p. 1105.
- [5] Alili, B., Bradai, D., Mathon, M. H., Jakani, S., Baudin, T.: *Kovove Mater.* 46, 2008, p. 371.
- [6] Tirsatine, K., Azzeddine, H., Baudin, T., Helbert, A. L., Brisset, F., Allili, B., Bradai D.: *J. Alloys. Compd.*, 610, 2014, p. 352.
- [7] Tirsatine, K., Azzeddine, H., Baudin, T., Helbert, A. L., Brisset, F., Bradai D.: *Mater. Eng.*, 24, 2017, p. 56.
- [8] Tirsatine, K., Azzeddine, H., Baudin, T., Helbert, A. L., Brisset, F., Bradai, D.: *Mater. Sci. Forum*, 879, 2017, p. 744.
- [9] Azzeddine, H., Tirsatine, K., Baudin, T., Helbert, A. L., Mathon, M. H., Brisset, F., Bradai D.: *Indian J. Eng. Mater. Sci.*, 24, 2017, p. 35.
- [10] Shin, D. H., Park, J.J., Kim, Y. S., Park K. T.: *Mater. Sci. Eng. A*, 328, 2002, p.98.

- [11] Gupta, A. K., Maddukuri, T. S., Singh S. K.: *Prog. Mater Sci.*, *84*, 2016, p.403.
- [12] Sunil, B. R, Kumar, A.A., Kumar T. S. S., Chakkingal U.: *Mater. Sci. Eng., C 33*, 2013, p.1607
- [13] Rafizadeh, E., Mani, A., Kazeminezhad, M.: *Mater. Sci. Eng. A*, *515*, 2009, p. 162.
- [14] Lee, J.W., Park,J.J.:*J. Mater. Process. Technol.*, *130–131*, 2002, p. 208.
- [15] Krishnaiah, A., Chakkingal, U., VenugopalP.: *Scr.Mater.*, *52*, 2005, p. 1229.
- [16] Kumar, S.S.S., Raghu, T.: *Mater. Des.*, *57*, 2014, p. 114.
- [17] Krishnaiah, A., Chakkingal, U., Venugopal, P.: *Mater. Sci. Eng. A*, *410–411*, 2005, p. 337.
- [18] Kumar, S. S. S., Raghu, T.: *J. Mater. Process. Technol.*, *213*, 2013, p. 214.
- [19] Kumar, S. S. S., Raghu, T.: *Mater. Sci. Forum*, *667-669*, 2011, p. 523.
- [20] Wang, Z. S., Guan, Y. J., Wang, G. C., Zhong, C. K.: *J. Mater. Process. Technol.*, *215*, 2015, p. 205.
- [21] Park, J. J., Park, N. J.: *J. Mater. Process. Technol.*, *169*, 2005, p. 299.
- [22] Yoon, S. C., Krishnaiah, A., Chakkingal, U., Kim, H. S.: *Computational Materials Science 43*, 2008, p.641.
- [23] Bachmann, F., Hielscher, R., Schaeben, H.: *Solid. State. Phenom.*, *160*, 2010,p. 63.
- [24] Holm, E. A., Olmsted, D. L., Foiles, S. M.: *Scripta Mater.*, *63*, 2010, p. 905.
- [25] Murr, L.: *Scripta Metal*, *6*, 1972, p. 203.
- [26] Smallman, R., Dillamore, I., Dobson, P.: *Le Journal de Physique Colloques 27*, 1966, p.3.
- [27] HadjLarbi, F., Azzeddine, H., Baudin, T., Mathon, M.H., Brisset, F., Helbert, A. L., Kawasaki, M., Bradai, D., Langdon, T. G.: *J. Alloys Compd.*, *638*, 2015, p. 88.

- [28] Khereddine, A. Y., HadjLarbi, F., Azzeddine, H., Baudin, T., Mathon, M.H., Helbert, A. L., Kawasaki, M., Bradai, D., Langdon, T. G.: *J. Alloys Compd.*, 574, 2013, p. 361.
- [29] Humphreys, F. J., Hatherly, M.: *Recrystallization and Related Annealing Phenomena*, Second Edition, NY, USA Elsevier Science Inc, 2004.
- [30] Engler, O.: *Acta Mater.*, 48, 2000, p. 4827.
- [31] Bowen, A. W.: *Mat. Sci. and Tech.*, 6, 1990, p. 1058.
- [32] Sarma, V. S., Eickemeyer, J., Schultz, L., Holzapfel, B.: *Scripta Mater.*, 50, 2004, p. 953.
- [33] Kumar, S. S. S., Raghu, T.: *Materials and Design*, 57, 2014, p.114.
- [34] Khodabakhshi, F., Kazeminezhad, M., Kokabi, A. H.: *Mat. Sci. Eng. A*, 527, 2010, p. 4043.
- [35] Fong, K. S., Tan, M. J., Chua, B. W., Atsushi, D.: *Procedia CIRP* 26, 2015, p.449.
- [36] Zimina, M., Bohlen, J., Letzig, D., Kurz, G., Cieslar, M., Zrník, J.: *IOP Conf. Series: Materials Science and Engineering*, 63, 2014, 012078.
- [37] Bonnot, E., Helbert, A.L, Brisset, F., Baudin, T.: *Mat. Sci. Eng. A*, 561, 2013, p. 60.
- [38] Estrin, Y.: *J. Mater. Process. Technol.*, 80, 1998, p. 33.
- [39] Baik, S. C., Estrin, Y., Kim, H. S., Hellmig, R. J.: *Mater. Sci. Eng. A*, 351, 2003 , p. 86.
- [40] Hosseini, E., Kazeminezhad, M.: *Int. J. Refract. Met.Hard. Mater.*, 27, 2009, p.605.
- [41] Hosseini, E., Kazeminezhad, M.:*Comput. Mater. Sci.*, 44, 2009, p. 962.
- [42] Hosseini, E., Kazeminezhad, M.:*Comput.Mater. Sci.*, 44, 2009, p. 1107.

[43] Kocks, U. E.: Texture and Anisotropy: Preferred Orientations in Polycrystals and Their Effect on Materials Properties, Cambridge University Press, 1998.

[44] Niranjana, G. G., Chakkingal, U.: J. Mater. Process. Technol., 210, 2010, p. 1511.

Table 1: Chemical composition of the Ni-14W (wt. %) alloy.

W	C	Mn	Mg	S	Ti
14	0.016	0.023	0.0017	<0.0005	<0.001

Table 2: Main ideal rolling texture components of FCC alloys.

Component	{hkl}<uvw>	Euler Angle		
		φ_1	ϕ	φ_2
□ Brass	{110}<112>	35°	35°	45°
◇ Goss	{110}<001>	0°	45°	0°
● Cube	{001}<100>	0°	0°	0°
△ Copper	{112}<111>	90°	35°	45°
▽ S	{231}<346>	59°	29°	63°

Figure captions

Fig. 1: Schematic illustration of the sequences of the groove pressing. Pressing with grooved (Figs. 1a and c) and flat (Figs. 1b and d) dies. An additional CCW 45° rotation around ND is applied between successive cycles after step d.

Fig. 2: IPF maps showing the microstructures of Ni-14W alloy: a) series I and b) series II.

Fig. 3: Histograms of the grain boundary misorientation angles of Ni-14W alloy: a) series I and b) series II.

Fig. 4: ODF sections at $\varphi_2 = 0, 45$ and 65° of Ni-14W alloy: a) series I and b) series II.

Fig. 5: IPF maps showing the microstructure evolution of the series I and II of Ni-14W alloy after GP processing up 4 cycles, respectively.

Fig. 6: Histograms of the misorientation angles of Ni-14W alloy after GP processing: a) series I and b) series II.

Fig. 7: Evolution of the grain size parameters and HAGB of Ni-14W alloy after GP processing: a) series I and b) series II.

Fig. 8: ODF sections at $\varphi_2 = 0, 45$ and 65° of Ni-14W alloy after GP processing up 4 cycles: a) series I and b) series II.

Fig. 9: Evolution of β and θ -fibre of Ni-14W alloy after GP processing up 4 cycles: (a, b) series I and (c, d) series II.

Fig. 10: Microhardness evolution of Ni-14W alloy after GP processing up to 4 cycles.

Fig. 11: Evolution of R value versus angle to rolling direction corresponding to experimental textures of GP processed samples: a) Series I and b) series II.

Fig. 12: Average Lankford factor \bar{R} and planar anisotropy ΔR versus number of GP cycles for both initial state of Ni-14W alloy.

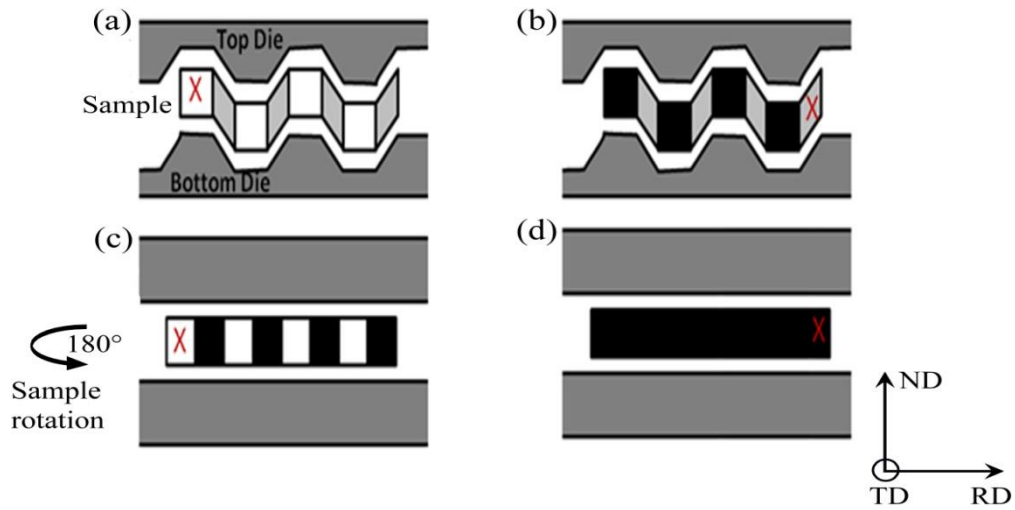


Fig. 1: Schematic illustration of the sequences of the groove pressing. Pressing with grooved (Figs. 1a and c) and flat (Figs. 1b and d) dies. An additional CCW 45° rotation around ND is applied between successive cycles after step d.

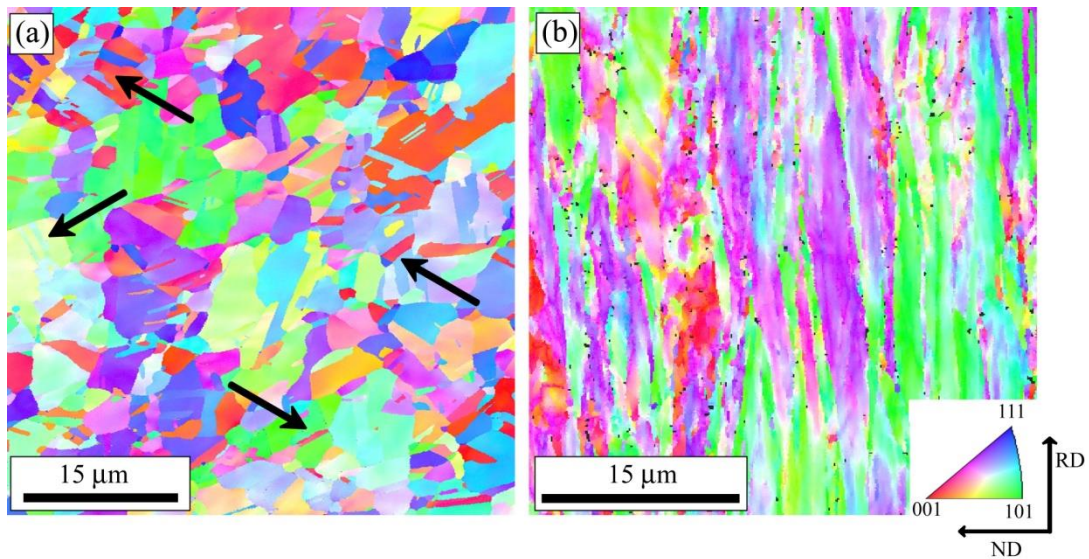


Fig. 2: IPF maps showing the microstructures of Ni-14W alloy: a) series I and b) series II.

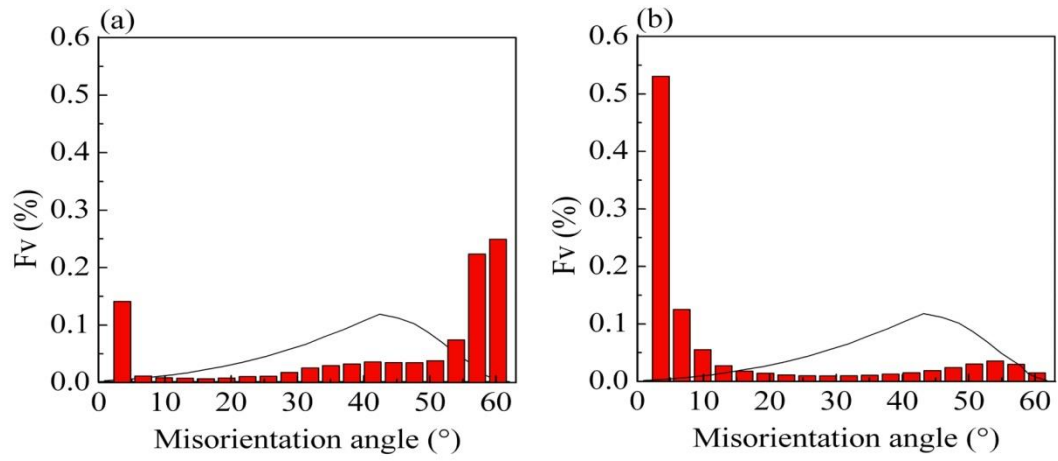


Fig. 3: Histograms of the grain boundary misorientation angles of Ni-14W alloy: a) series I and b) series II.

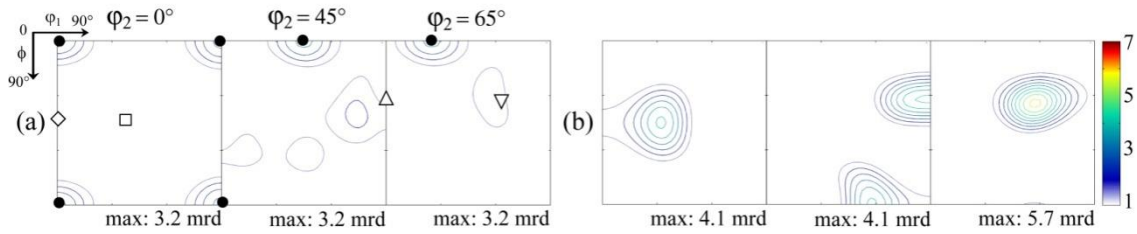


Fig. 4: ODF sections at $\phi_2 = 0, 45$ and 65° of Ni-14W alloy: a) series I and b) series II.

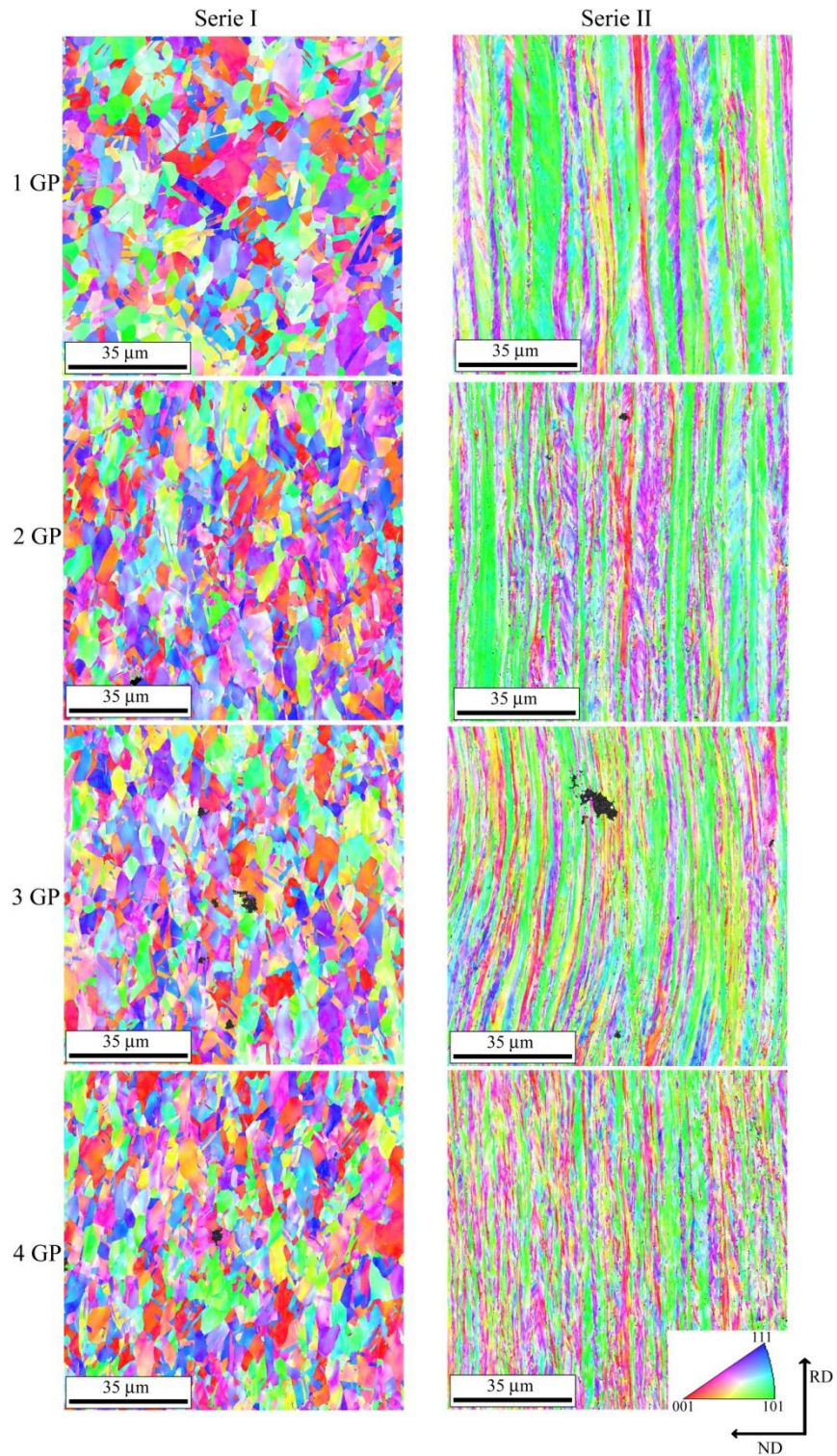


Fig. 5: IPF maps showing the microstructure evolution of the series I and II of Ni-14W alloy after GP processing up 4 cycles, respectively

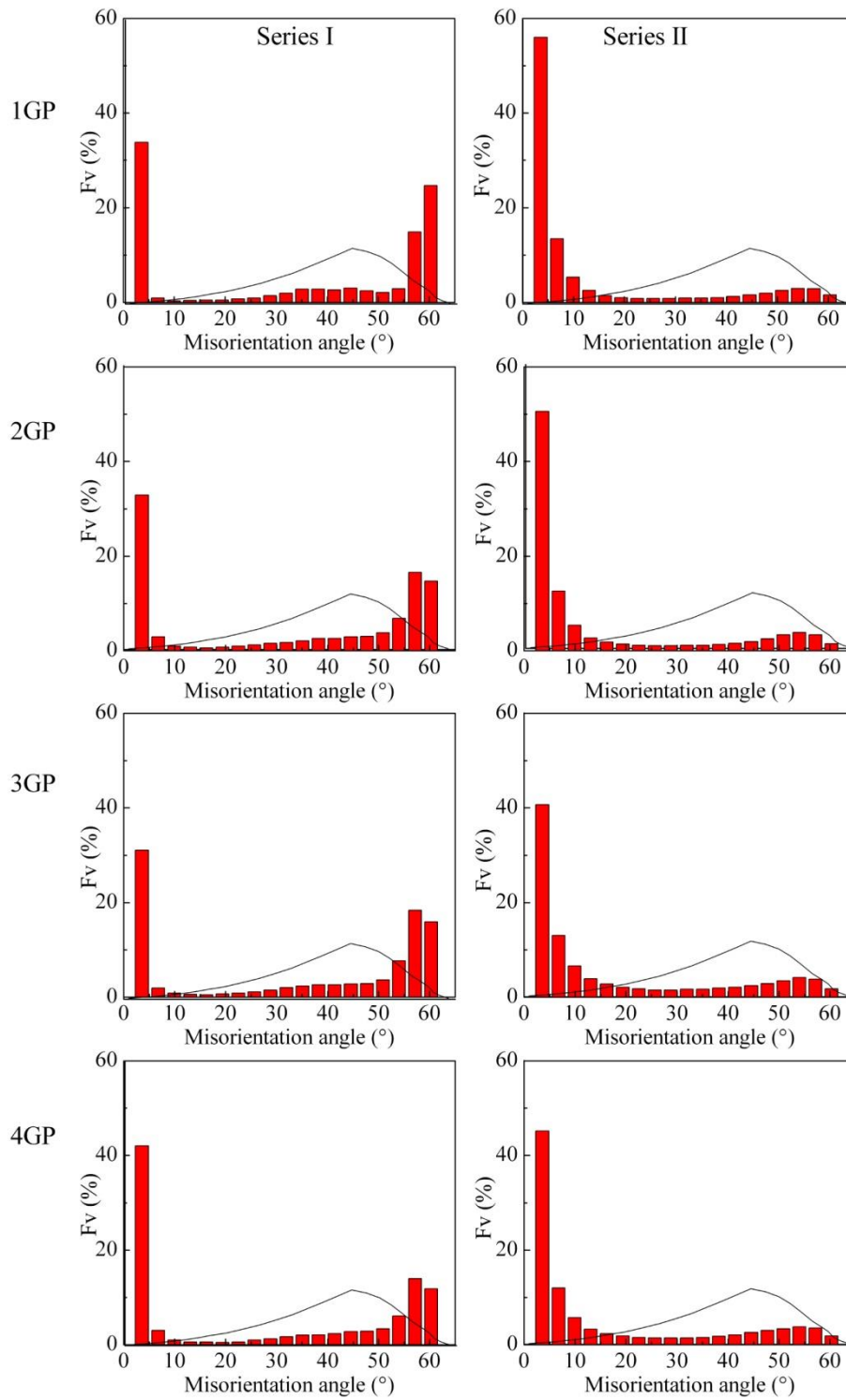


Fig.6:Histograms of the misorientation angles of Ni-14W alloy after GP processing: a) series I and b) series II.

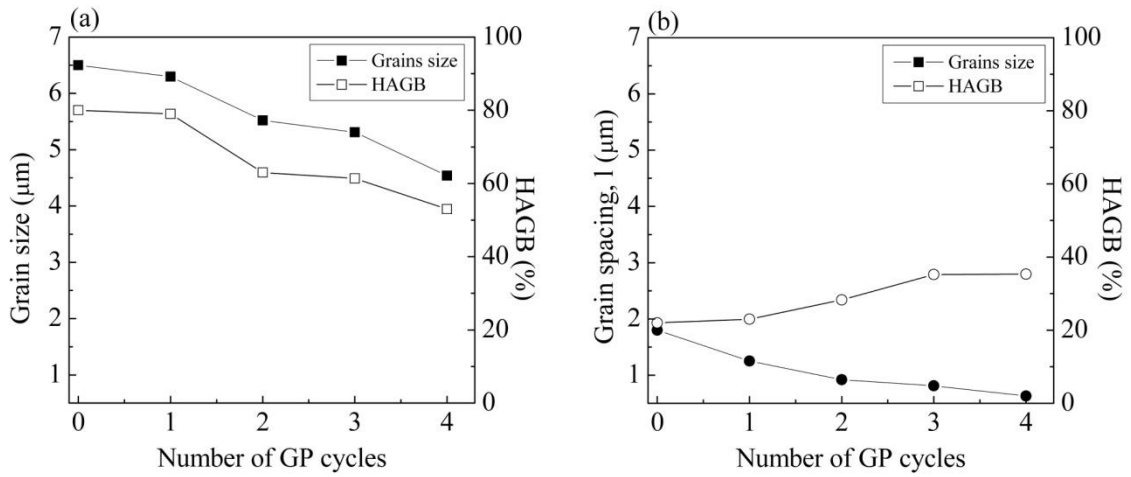


Fig.7: Evolution of the grain size parameters and HAGB of Ni-14W alloy after GP processing: a) series I and b) series II.

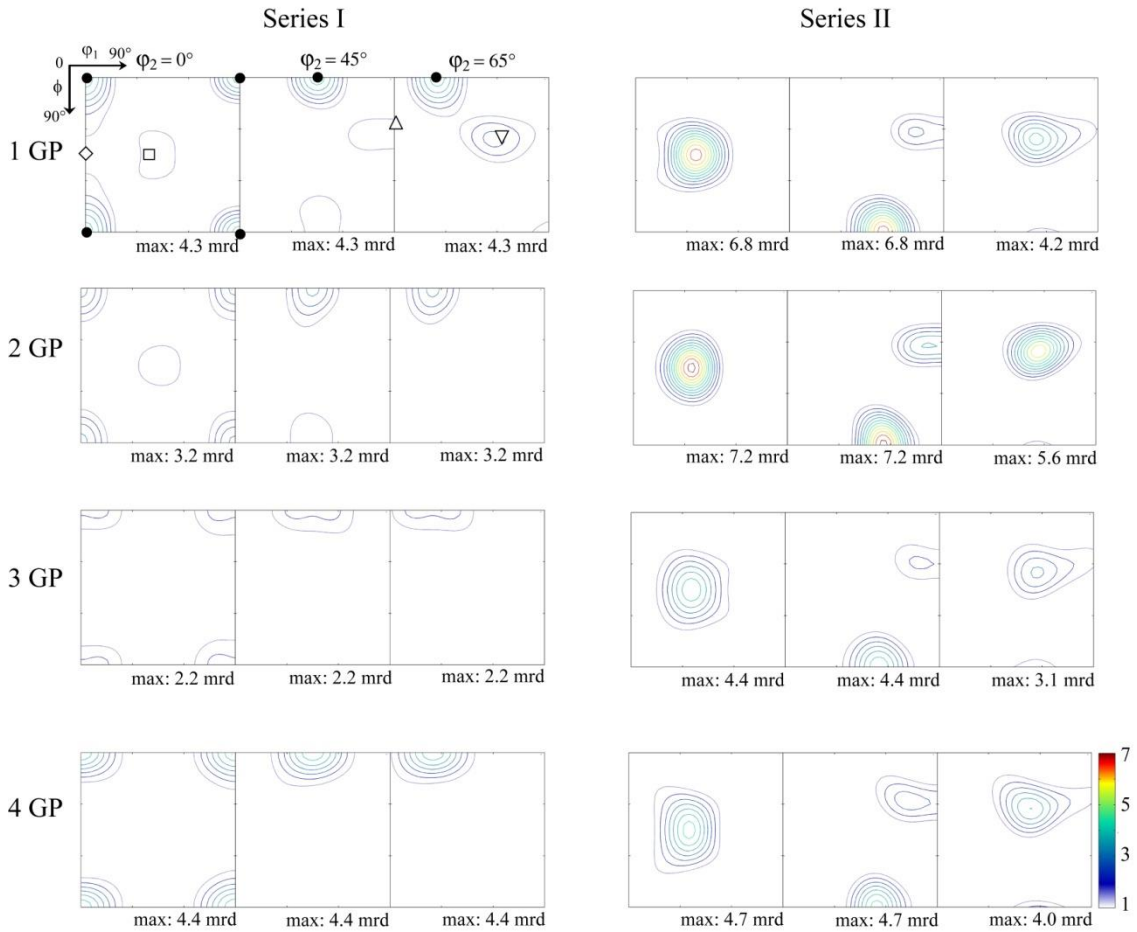


Fig. 8: ODF sections at $\phi_2 = 0, 45$ and 65° of Ni-14W alloy after GP processing up to 4 cycles: a) series I and b) series II.

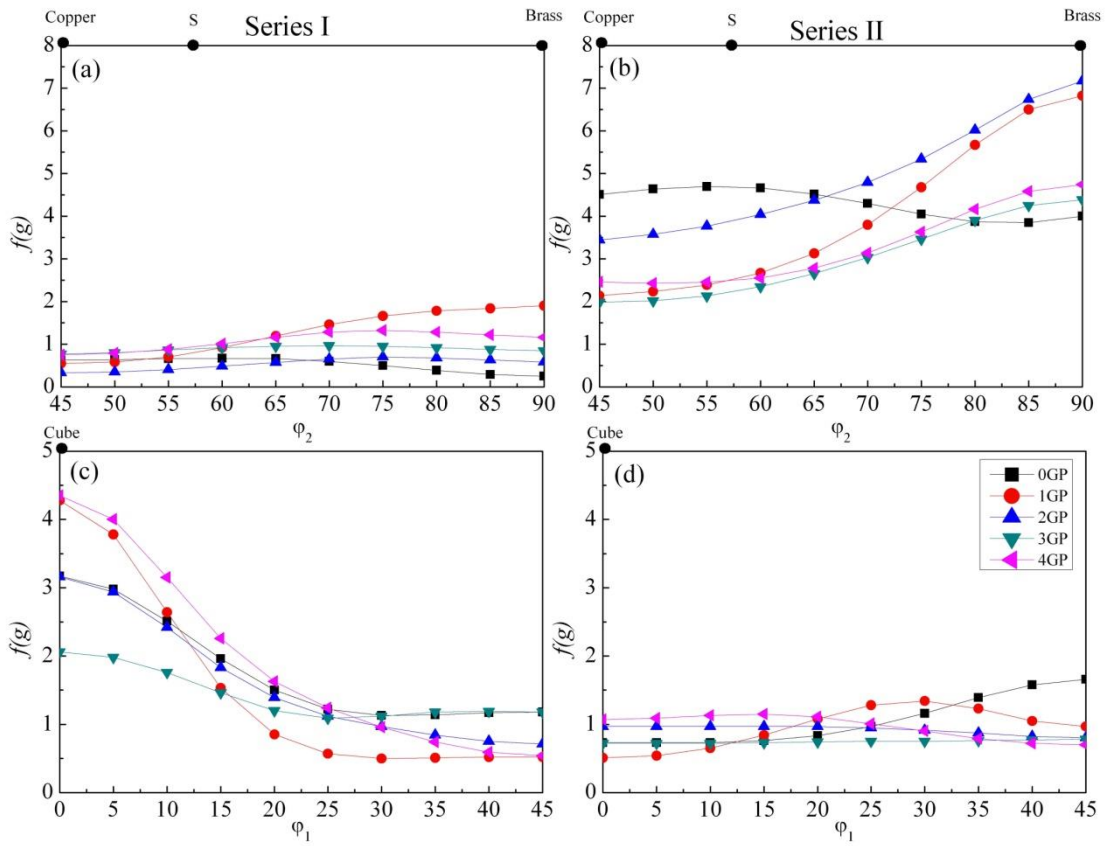


Fig.9:Evolution of β and θ -fibre of Ni-14W alloy after GP processing up to 4 cycles: (a, b) series I and (c, d) series II.

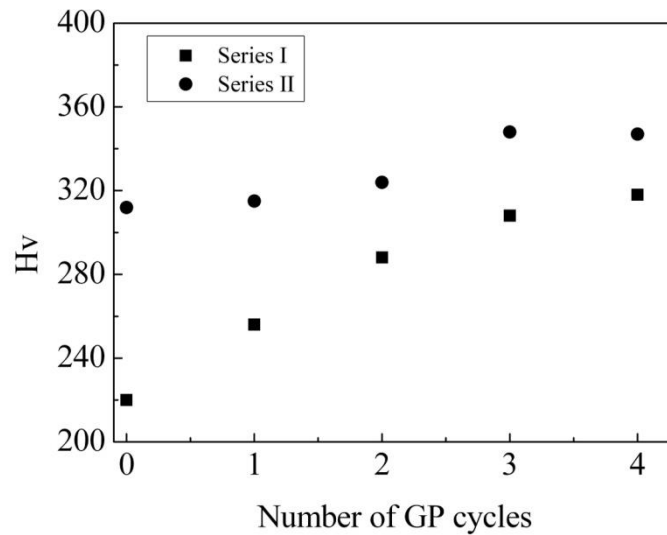


Fig. 10:Microhardness evolution of Ni-14W alloy after GP processing up to 4 cycles.

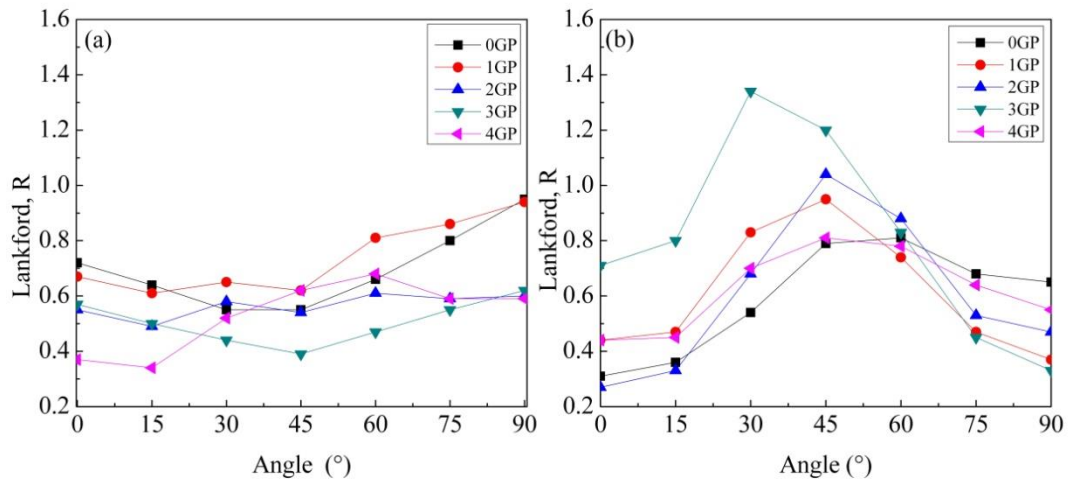


Fig. 11: Evolution of R value versus angle to rolling direction corresponding to experimental textures of GP processed samples: a) Series I and b) series II.

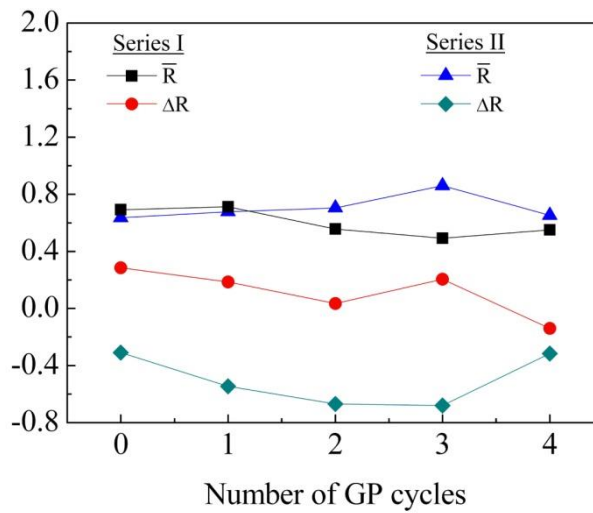


Fig. 12: Average Lankford factor \bar{R} and planar anisotropy ΔR versus number of GP cycles for both initial state of Ni-14W alloy.